PNAS

Supplementary Information for
Longitudinal *In Vivo* Ca^{2+} Imaging Reveals Dynamic Activity Changes of Diseased Retinal Ganglion Cells at Single-Cell Level

Liang Li[a,1], Xue Feng[a,1], Fang Fang[a,b,1], David A Miller[c], Shaobo Zhang[d], Pei Zhuang[a], Haoliang Huang[a], Pingting Liu[a], Junting Liu[a], Nripun Sredar[a], Liang Liu[a], Yang Sun[a], Xin Duan[d], Jeffrey L Goldberg[a], Hao F Zhang[c], and Yang Hu[a,2]

[2]Corresponding author: Yang Hu, Email: huyang@stanford.edu

This PDF file includes:

Supplementary text

Figures S1 to S6

Legends for Movies S1 to S3

Other supplementary materials for this manuscript include the following:

Movies S1 to S3

Supplementary Materials and Methods

Reagents and Softwares

Reagent type (species) or resource	Designation	Source or reference	Identifiers	Dilution
strain, strain background (Mus musculus)	C57BL/6J	Jackson Laboratories	000664	
strain, strain background (Mus musculus)	B6N.129-Rpl22tm1.1Psam/J	Jackson Laboratories	011029	
antibody	anti-RBPMS (guinea pig polyclonal)	Custom-made by ProSci		1:4000
antibody	Anti-GFP (chicken) IgY	Aves Lab/Fisher	GFP-1010	1:500
antibody	Anti-ChAT (goat)	Millipore	MAB305	1:500
antibody	Anti-3HA (rat)	Roche	11867423001	1:200
antibody	Anti-VAChT (goat)	EMD Millipore/ Fisher	ABN100	1:500
antibody	Anti-AP2α	Developmental Studies Hybridoma Bank	3B5	1:100
antibody	Alexa Flour647 Donkey anti-Guinea Pig IgG	Jackson ImmunoResearch	706-605-148	1:200

antibody	Cy3 Donkey anti-goat IgG	Jackson ImmunoResearch	705-165-147	1:200
antibody	Alexa Flour 488 Donkey anti-Chicken IgY (IgG)	Jackson ImmunoResearch	703-545-155	1:200
antibody	Cy3 Goat anti-rat IgG	Jackson ImmunoResearch	112-165-167	1:200
antibody	Cy3 Goat anti-mouse IgG	Jackson ImmunoResearch	112-165-166	1:200
chemical compound, drug	Silicone oil	Alcon Laboratories	1,000 mPa.s, Silikon	
software, algorithm	Graphpad prism7	GraphPad Software		
software, algorithm	Volocity software	Quorum Technologies		
software, algorithm	ImageJ/Fiji	NIH		
software, algorithm	MATLAB	Mathworks		

Constructs and AAV production. The coding region of jGCaMP7s (Addgene, #104487) was cloned into the pAM-AAV-mSncg-GFP-WPRE backbone with EcoRI and MluI sites, driven by RGC-specific mSncg promoter (1). The pAM-AAV-mSncg-Cre plasmid was also constructed using the same strategy. The maxi-precipitation of the constructs was performed by following the manual of Endo-Free Plasmid Maxi kit (Omega Bio-tek, D6926-03/101319-342). The detailed procedure of the AAV production has been described previously (1). Briefly, AAV plasmids containing the jGCaMP7s or Cre were co-transfected with pAAV2 (pACG2)-RC triple mutant (Y444, 500, 730F) and the pHelper

plasmid (Stratagene) into HEK293T cells by the polyjet (SignaGen Laboratories, SL100688) transfection reagent. The cells were lysed to release the viral particles 72 hours after transfection, which were precipitated by 40% polyethylene glycol and purified by two rounds of cesium chloride density gradient centrifugation. The virus bands were taken out for dialysis in a MWCO 7000 Slide-A–LYZER cassette (Pierce) overnight at 4°C. The AAV titers of jGCaMP7s and Cre were determined by real-time PCR and diluted to 4.5 x 10^{12} and 1.5 x 10^{11} vector genome (vg)/ml for intravitreal injection, respectively.

Intravitreal injection. Mice were anesthetized by xylazine and ketamine based on their body weight (0.01mg xylazine/g + 0.08mg ketamine/g). For AAV intravitreal injection, a pulled and polished microcapillary tube was inserted into the peripheral retina of 4-week-old mice just behind the ora serrata. Approximately 2 µl of the vitreous was removed to allow injection of 2 µl AAV into the vitreous chamber. The mice were housed for an additional 4 weeks after AAV injection to achieve stable jGCaMP7s expression.

***In vivo* RGC Ca^{2+} imaging by cSLO.** The custom-made UV ring light (Shanghai Fugen Automation Technology Co., Ltd, FG-DR90-A45-UV, 395nm, diameter: 90mm, angle 45º) was mounted on the 55º lens of the Spectralis cSLO (Heidelberg Engineering GmbH, Heidelberg, Germany) and controlled by an Arduino module (www.arduino.cc) that is programmed to control light onset and offset. Both the Arduino module and cSLO were controlled by the same foot pedal through a XLR 3-pin Y cable cord, to ensure the synchronization of UV light stimulation and Ca^{2+} signal recording. The Arduino module code of light stimulation (https://github.com/HuLab-Code/SynchronizeUVSpectralis) was

editable for start time, onset/offset duration and cycles. The output power of the UV light was 3.5 mW measured by power meter (Newport, Model 1919-R) and the UV power received by the fundus of adult mouse retina was ~32 μW, measured *ex vivo* from a mounted half eyeball (mean of 7 eyes). For *in vivo* Ca^{2+} imaging: the mouse was anesthetized by xylazine and ketamine as previously described after dark adaptation for 30 minutes. Mydriasis and cycloplegia were achieved by applying a drop of 1% tropicamide solution and a drop of 2.5% phenylephrine hydrochloride solution, which prevents pupillary contraction during recording. The anesthetized mouse was placed on a 3D-printed mouse holder with a 37ºC heater, and a custom-made +10D mouse contact lens (3.0 mm diameter, 1.6 mm BC, PMMA clear, Advanced Vision Technologies) was attached to keep the cornea from drying. The mouse retinal fundus was imaged by a 55º lens with fluorescein angiography scanning mode of the cSLO under the same sensitivity (sensitivity 75-85), at 4.7 frames/s imaging frequency and high-resolution mode (1536 x 1536 pixels) for a maximum movie recording time (60s). The 488 nm excitation light used for GCaMP imaging was kept constant at 0.3 μW output laser power. The 60s recording cycle: 10 seconds before UV stimulation to obtain the basal level of fluorescence (*F0*), 20 seconds of full field UV light pulse stimulation, and 30 seconds after UV offset to obtain stimulation (ON/OFF)-induced fluorescence (*F*). During the Ca^{2+} imaging, the optic nerve head was centered and focus was on the GCL layer. Normally two recordings from the same eye with focus on the dorsal/temporal region and the ventral/nasal region were necessary to cover the whole fundus. At least 3 minutes of dark break between the two recordings allowed full recovery of light-evoked RGC activity. Antibacterial steroidal ophthalmic ointment (Neomycin. Akorn, Somerset, New Jersey) was applied at the end of recording.

It is important to note that full pupil dilation, clear cornea and lens, and focus are key factors for consistent longitudinal Ca^{2+} imaging. All Ca^{2+} imaging data was exported as an uncompressed video after eye-motion correction processed by the Heidelberg software. The x-y scale of the mouse fundus was calibrated by imaging 10 μm fluorescent Microspheres (Life Technologies, F8830) injected intravitreally.

Ca^{2+} imaging data analysis. MATLAB 2019b (The Mathworks Inc.) was used to perform most of the image data analysis as detailed below.

1. **RGC segmentation/regions of interest (ROI) detection and fluorescent signal extraction**: The eye-motion corrected Ca^{2+} imaging video was transformed from RGB to 8bit data and cropped 550 x 600 pixels (624 μm x 680 μm) at the nasal and temporal fundi, 550 x 500 pixels (624 μm x 567 μm) at the dorsal and ventral fundi by ImageJ-Fiji for further cell segmentation. A MATLAB algorithm was generated (RSE, https://doi.org/10.5281/zenodo.6842368) to identify cell ROIs using the following procedure: In each selected raw image (*I*), the original image was filtered with a 2-D Gaussian smoothing kernel (*imgaussfilt*) with sigma=20 pixels to get a blurred background image (*IF*), and the mean intensity (*IM*) of the raw image was calculated. Further, a binary image (*BW*) was generated through image thresholding with the following parameter: *BW= I>IF*1.25 & I > IM*. Then, *bwareaopen(BW,40)* was performed to remove connected components (objects) in the binary image with fewer than 40 pixels. Next, the ROIs from each selected image were detected and registered using *imfindcircles (2)* with a radius range from 5 to 15 pixels. Finally, registered ROIs from selected images were merged by

combining ROIs within 10 pixels of each other to determine individual RGC soma. The averaged center position and radius of the merged ROIs were assigned to the new ROIs of detected RGCs. Because different RGCs may show peak fluorescence intensity at different time frames due to their specific response dynamics to the visual stimulus, every 5^{th} image frame (about 1 second interval) was used to detect the ROIs. The mean RGC fluorescence intensities for all time points within the ROIs were then extracted as the raw fluorescence intensity for individual RGCs. To minimize the effect of background intensity change during recording, the blood vessel area was segmented from the maximum projection image through thresholding. The average intensity with respect to time within the segmented region was extracted as a reference background intensity. This background intensity signal was subtracted from the fluorescent intensity signals for each RGC to acquire the normalized fluorescence intensity (F) at a given time. A time series of fluorescent intensity ($F0$ was at the first 10 seconds before UV light stimulation and F was during the next 50 seconds after initial UV onset) from all segmented RGCs was then generated with an embedded stimulus time marker. Each neuronal response was normalized by subtracting the average signal intensity before UV stimulus, $F0$, from all time points and dividing the resulting signal by $F0$. This process can be summarized as $\Delta F/F0 = (F-F0)/F0$. Finally, the pooled RGCs' time series of neuronal responses ($\Delta F/F0$) was denoised by a low-pass filter (*lowpass*) below normalized passband frequency (0.3 π rad/sample) to remove high-frequency noise before further clustering and grouping.

2. **Functional RGC unsupervised clustering and hierarchical grouping:** The clustering and grouping procedures that we developed and detail below were based on previously described principles and protocols (3). First, we determined the range of non-specific fluctuation of fluorescence intensity in *in vivo* RGC imaging, which is in between +15% to -20% (*ΔF/F0*). Thus, we defined the RGCs with fluorescence changes within this range in response to UV stimulation as no-response (NR) RGCs. We then analyzed the rest of the RGCs with significant changes of fluorescence intensity in response to light stimulation using 6 unbiased sparse response features extracted by sparse principal component analysis (sPCA) (4, 5), and therefore resulted in a 6-dimensional feature vector for each RGC. We fit each data set with a Gaussians mixture distribution model using an iterative expectation-maximization (EM) algorithm (MATLAB's *fitgmdist* object) (6) with a maximum of 2000 optimization iterations. In the setup, we constrained the covariance matrix for each component to be diagonal, resulting in 12 parameters per component (6 for the mean, 6 for the variances). To avoid local minima, we set the EM algorithm repeating 20 times per candidate number of clusters and used the solution with the greatest likelihood. To find the optimal number of clusters, we evaluated the Bayesian information criterion (BIC) (7), which resulted in 40 automatically defined RGC clusters. These RGC clusters were further re-grouped with a custom-made one-dimensional hierarchical clustering MATLAB script (RCC, https://doi.org/10.5281/zenodo.6842355) to combine similar clusters to achieve a good compromise between clustering complexity and quality. In this step, we used the unweighted average distance (UPGMA) algorithm to calculate the standard

linkage (*linkage*) of the means of the RGC clusters and obtain the correlation distance. We presented the linkage result as a dendrogram plot (using *linkage* and *dendrogram*). The leaf order was optimized using the MATLAB's *optimalleaforder* function and modified for clarity of presentation. By setting the grouping distance threshold as 0.28, 9 RGC functional groups were identified based on their similarity as presented in the main manuscript and the grouped individual data points were projected to a two-dimensional space by using t-Distributed Stochastic Neighbor Embedding (*tSNE*) (8) for visualization. For the clustering analysis under different conditions, each detected RGC fluorescent signal trace was normalized by its Euclidean norm (*norm* function) and compared with the normalized mean intensity of each group by performing the cross-correlation (*xcross* function in MATLAB, with lag range set as 0). The RGC trace was then assigned to the group that has the highest cross-correlation value that is larger than 0.75.

3. **Referencing correlation fitting:** For RGC clustering analysis in disease models, each detected RGC fluorescent signal trace was normalized by its Euclidean norm (*norm* function) and compared with the normalized mean intensity of each group by performing the cross-correlation (*xcross* function in MATLAB, with lag range set as 0). The RGC trace was then assigned to the group that has the highest cross-correlation value that is larger than 0.75. The RGC group assignment based on the 9 RGC functional groups was performed with a custom-made RGC referencing clustering MATLAB script (RRC, https://doi.org/10.5281/zenodo.6842364).

4. **Amplitude quantification:** The signal amplitude was quantified based on the group into which the trace was classified. For ON-Sust1, ON-Sust2, and ON-Trans signals, the amplitude was defined as the difference between the baseline signal intensity before stimulus onset and the peak signal intensity after stimulus onset. For ON-Sust3, the amplitude was defined as the difference between the peak intensity after stimulus onset to the minimum intensity after stimulus offset. The amplitudes of the two peaks of ON-OFF signals were measured individually and averaged to generate the mean amplitudes. For OFF-Trans and OFF-Sust signals, the amplitude was defined as the intensity difference at F0 to the peak after stimulus offset. For OFF-SS 1/2 signals, the amplitude was defined as the difference between the baseline signal intensity before stimulus onset and the lowest signal intensity at stimulus offset.

Optic nerve crush (ONC). ONC was performed 4 weeks following AAV injection to mice at about 8-9 weeks of age (9-11): the optic nerve was exposed intraorbitally while care was taken not to damage the underlying ophthalmic artery, and crushed with a jeweler's forceps (Dumont #5; Fine Science Tools, Foster City, California) for 5 seconds approximately 0.5 mm behind the eyeball. Eye ointment containing neomycin (Akorn, Somerset, New Jersey) was applied to protect the cornea after surgery. RGC Ca^{2+} imaging of the same fundus region was acquired at 0, 1, 3, 5, 7, and 14 days post crush (dpc) by cSLO.

SOHU glaucoma model and IOP measurement. The detailed procedure has been published before (12-14). In brief, 9-week-old mice were anesthetized by an intraperitoneal injection of Avertin (0.3mg/g) before a tunnel was made by a 32G needle through the layers of the cornea at the superotemporal side close to the limbus to reach the anterior chamber without injuring lens or iris. Then, ~ 2μl silicone oil (1,000 mPa.s, Silikon, Alcon Laboratories, Fort Worth, Texas) was injected slowly into the anterior chamber using a homemade sterile glass micropipette, until the oil droplet expanded to cover most areas of the iris (diameter ~ 1.8-2.2mm). After the injection, veterinary antibiotic ointment (BNP ophthalmic ointment, Vetropolycin, Dechra, Overland Park, Kansas) was applied to the surface of the injected eye. The contralateral control eyes received 2μl normal saline to the anterior chamber. During the whole procedure, artificial tears (Systane Ultra Lubricant Eye Drops, Alcon Laboratories, Fort Worth, Texas) were applied to keep the cornea moist. The IOP of both eyes was measured by the TonoLab tonometer (Colonial Medical Supply, Espoo, Finland) according to product instructions. Briefly, in the morning, mice were anesthetized with a sustained flow of isoflurane (3% isoflurane at 2 L/minute mixed with oxygen) delivered to the nose by a special rodent nose cone (Xenotec, Inc., Rolla, Missouri), which left the eyes exposed for IOP measurement. 1% Tropicamide Sterile Ophthalmic solution (Akorn, Somerset, New Jersey) was applied three times at 3-minute intervals to fully dilate the pupils (about 10 minutes) before taking measurements. The average of six measurements by the TonoLab was considered as one machine-generated reading and three machine-generated readings were obtained from each eye; the mean was calculated to determine the IOP. During this procedure, artificial tears were applied to keep

the cornea moist. The Ca^{2+} imaging, OCT, and PERG were performed at the same time points (0, 0.4, 1, 3, 5, 8wpi).

Immunohistochemistry of retinal wholemounts; RGC counts. After transcardiac perfusion with 4% PFA in PBS, the eyes were dissected out, post-fixed with 4% PFA for 2 hours at room temperature, and cryoprotected in 30% sucrose overnight. Retinas were then dissected out and washed extensively in PBS before blocking in staining buffer (10% normal donkey serum and 2% Triton X-100 in PBS) for 30 minutes. RBPMS guinea pig antibody (ProSci, California), GFP chicken antibody (Aves Lab, GFP-1010), choline acetyltransferase (ChAT)/ vesicular acetylcholine transporter (VAChT) goat antibody (EMD Millipore) and AP2α mouse antibody were used at 1:4000, 1:500, 1:500 and 1:100 to label RGCs, jGCaMP7s^{+}, and amacrine cells, respectively. Floating retinas were incubated with primary antibodies overnight at 4°C and washed 3 times for 30 minutes each with PBS. Secondary antibodies (Alexa Fluor 647-donkey anti-guinea pig, Alexa Fluor 488-donkey anti-chicken, Cy3-donkey anti-goat and Cy3-goat anti-mouse) were then applied (1:200; Jackson ImmunoResearch, West Grove, Pennsylvania) and incubated for 1 hour at room temperature. Retinas were again washed 3 times for 30 minutes each with PBS before a cover slip was attached with Fluoromount-G (Southernbiotech, Birmingham, Alabama). Images of immunostained wholemounts were acquired with a Zeiss confocal microscope (LSM 880) with 20x and 40x oil lens and serial filters (BP410-510 for DAPI, BP520-550 for Alexa Fluor 488, BP565-650 for Cy3 and BP650-750 for Alexa Fluor 647). To measure RGC neurites, confocal images of wholemount retinas were obtained with a 40x lens in 1 μm optical sections and a 1.5 μm interval in Z stacking mode. For RGC

counting, 6-9 fields were randomly sampled from peripheral regions of each retina using a 40x lens and a Zeiss M2 epifluorescence microscope, and $RBPMS^+$ RGCs counted by Volocity software (Quorum Technologies). The percentage of RGC survival was calculated as the ratio of surviving RGC numbers in injured eyes compared to contralateral uninjured eyes. The investigators who counted the cells were blinded to the treatment of the samples. For cross sections of retina, the eyes were dehydrated in 30% sucrose solution overnight before embedding in OCT on dry ice. Serial cross sections (14 μm) were cut with a Leica cryostat and collected on Superfrost Plus Slides and stored at –80°C until processed. Cryosections of eyes were prepared for the immunostaining procedures and images acquired by Zeiss confocal microscope (LSM 880) with 40x oil lens.

ON semi-thin sections and quantification of surviving axons. The detailed procedure has been described previously (9, 13). Briefly, transverse semi-thin (1 μm) sections of ON were cut on an ultramicrotome (EM UC7, Leica, Wetzlar, Germany) from tissue collected 2 mm distal to the eye (about 1.5 mm distal to the crush site), and stained with 1% para-phenylenediamine (PPD) in methanol: isopropanol (1:1). Four sections of each ON were imaged through a 100x lens of a Zeiss M2 epifluorescence microscope to cover the entire area of the ON without overlap. Two areas of 21.4 μm X 29.1 μm from the center of each image were cropped, and counted manually with ImageJ. After counting all the images taken from a single nerve, the mean of the surviving axon number was calculated for each ON, and compared to that in the contralateral control ON to yield a percentage of axon survival value. The investigators who counted the axons were masked to the treatment of the samples.

Spectral-domain optical coherence tomography (SD-OCT) imaging. At the conclusion of Ca^{2+} imaging, fundus OCT imaging was performed under OCT mode by switching to a 30º licensed lens (Heidelberg Engineering) as in the previously described procedure (13, 15). Briefly, the mouse retina was scanned with the ring scan mode centered by the ON head at 100 frames average under high-resolution mode (each B-scan consisted of 1536 A scans). The ganglion cell complex (GCC) includes retinal nerve fiber layer (RNFL), ganglion cell layer (GCL), and inner plexiform layer (IPL). The average thickness of GCC around the ON head was measured manually with the Heidelberg software. The mean of the GCC thickness in the injured retina was compared to that in the contralateral control retina to yield a percentage of GCC thickness value. The investigators who measured the thickness of GCC were blinded to the treatment of the samples.

Pattern electroretinogram (PERG) recording. PERG recording of both eyes was performed at the same time with the Miami PERG system (Intelligent Hearing Systems, Miami, FL), as described in our previous publication (13, 15). In brief, a feedback-controlled heating pad (TCAT-2LV, Physitemp Instruments Inc., Clifton, New Jersey) maintained animal core temperature at 37°C. A small lubricant eye drop (Systane) was applied before recording to prevent corneal opacities. The reference electrode was placed subcutaneously on the back of the head between the two ears, the ground electrode was placed at the root of the tail, and the active steel needle electrode was placed subcutaneously on the snout for the simultaneous acquisition of left and right eye responses. Two 14 cm x 14 cm LED-based stimulators were placed in front so that the

center of each screen was 10 cm from each eye. The pattern remained at a contrast of 85% and a luminance of 800 cd/m^2, and consisted of four cycles of black-gray elements, with a spatial frequency of 0.052 c/d. Upon stimulation, the independent PERG signals were recorded from the snout and simultaneously by asynchronous binocular acquisition. With each trace recording up to 1020 ms, two consecutive recordings of 200 traces were averaged to achieve one readout. The first positive peak in the waveform was designated as P1 and the second negative peak as N2. P1 was typically around 100 ms. The mean amplitude of the P1-N2 amplitude in the injured eye was compared to that in the contralateral control eye to yield a percentage of amplitude change. The investigators who measured the amplitudes were blinded to the treatment of the samples.

OKR measurement. The spatial vision of both eyes was measured using the opto-kinetic response (OKR) as described in our previous publication (13, 15). In brief, living mice were placed unrestrained on a platform in the center of four 17-inch LCD computer monitors (Dell, Phoenix, AZ); their movement was captured by a video camera above the platform. A rotating cylinder with vertical sine wave grating was computed and projected to the four monitors by OptoMotry software (CerebralMechanics Inc., Lethbridge, Alberta, Canada). The sine wave grating provides a virtual-reality environment to measure the spatial acuity of left eye when rotated clockwise and right eye when rotated counterclockwise. When the mouse calmed down and stopped moving, the gray of the monitor immediately switched to a low spatial frequency (0.1 cycle/degree) for five seconds, in which the mouse was assessed by judging whether the head turned to track the grating. The short time frame of assessment ensured that the mice did not adapt to the

stimulus, which would lead to false readouts. The mice were judged to be capable of tracking the grating. The spatial frequency was increased repeatedly until a maximum frequency was identified and recorded. The % of vision acuity was yielded by comparing the maximum frequency of the experimental eye to that of the contralateral eye. The mice were tested in the morning and the investigator who judged the OKR was blinded to the treatment of the mice.

Neurite tracing. Confocal images of RGCs labeled for GFP and RBPMS were taken with 1 μm optical sections and 1.5 μm intervals of the Z stacking mode from the GCL to IPL layers. The GFP/jGCaMP7s-labeled neurites of naïve, ONC and SOHU RGCs were traced, outlined and calculated in the z stack images via the simple neurite tracer (SNT) plugin of the ImageJ/Fiji (https://imagej.net/SNT).

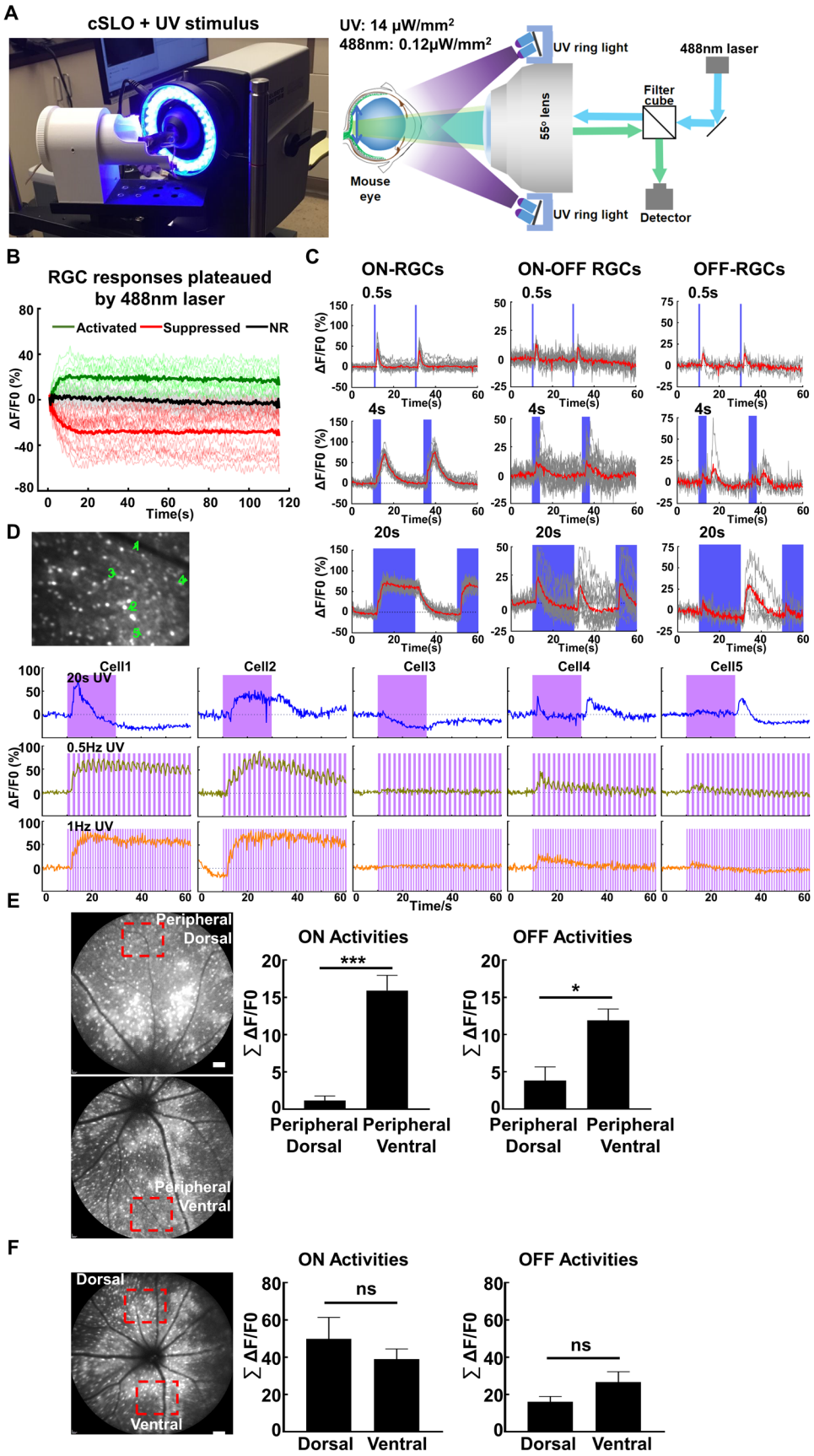
A
cSLO + UV stimulus
UV: 14 μW/mm²
488nm: 0.12μW/mm²
UV ring light
488nm laser
Filter cube
55° lens
Mouse eye
UV ring light
Detector
B
RGC responses plateaued by 488nm laser
Activated
Suppressed
NR
ΔF/F0 (%)
Time(s)
C
ON-RGCs
ON-OFF RGCs
OFF-RGCs
0.5s
4s
20s
D
Cell1
Cell2
Cell3
Cell4
Cell5
20s UV
0.5Hz UV
1Hz UV
Time/s
E
Peripheral Dorsal
Peripheral Ventral
ON Activities
OFF Activities
∑ ΔF/F0
***
*
Peripheral Dorsal
Peripheral Ventral
F
Dorsal
Ventral
ON Activities
OFF Activities
ns
Dorsal
Ventral

Fig. S1. Optimization of *in vivo* Ca^{2+} imaging by customized cSLO of mouse RGCs labeled with jGCaMP7s. (**A**) Schematic of customized Heidelberg cSLO with synchronized UV light for mouse *in vivo* Ca^{2+} imaging. The fundus of adult mouse eye receives ~ 14 μW/mm^2 of UV and ~ 0.12 μW/mm^2 of 488nm excitation light. (**B**) The RGCs' responses to 488 nm imaging light plateau after 20 seconds. n = 47 RGCs from one retina. (**C**) The grey waveform traces are the responses of individual RGCs (ΔF/F0) to UV light stimulation for 0.5, 4 or 20 seconds, as the function of time clustered in three typical RGC functional groups. Red line is the mean. (**D**) The mean waveforms of five representative RGCs from the same retina in response to UV light stimulation for 20 seconds once, at 0.5 or 1Hz for multiple cycles during the 60 seconds recording cycle. **(E)** *In vivo* Ca^{2+} imaging of peripheral dorsal and ventral RGCs. Data are presented as means ± s.e.m, n = 4 retinas. *: $p<0.05$, ***: $p<0.001$. Student's t-test. **(F)** *In vivo* Ca^{2+} imaging of fundus dorsal and ventral RGCs. Data are presented as means ± s.e.m, n = 8 retinas. ns: no significance. Student's t-test.

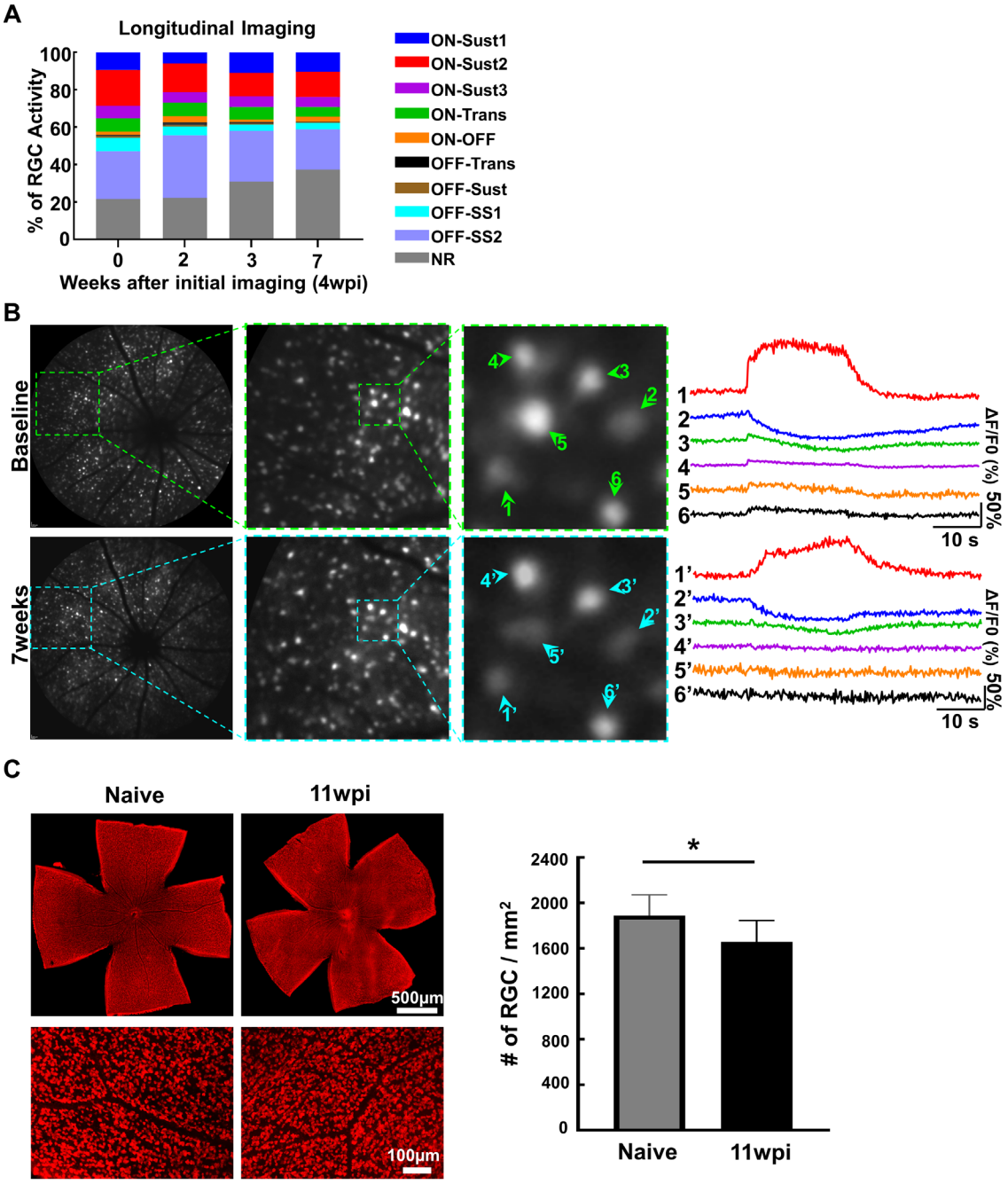

Fig. S2. Quantification of naïve RGCs' activities over time by longitudinal Ca^{2+} imaging. (**A**) Percentages of 9 RGC activity groups at different time points, detected by longitudinal Ca^{2+} imaging and clustering. (**B**) Examples of longitudinal single RGC Ca^{2+} imaging tracing at baseline (4wpi) and 7 weeks later. (**C**) RGC numbers in naïve mouse

retinas and mouse retinas injected with AAV-jGCaMP7s for 11 weeks. Data are presented as means ± s.e.m, n = 5. *: $p<0.05$. Student's t-test.

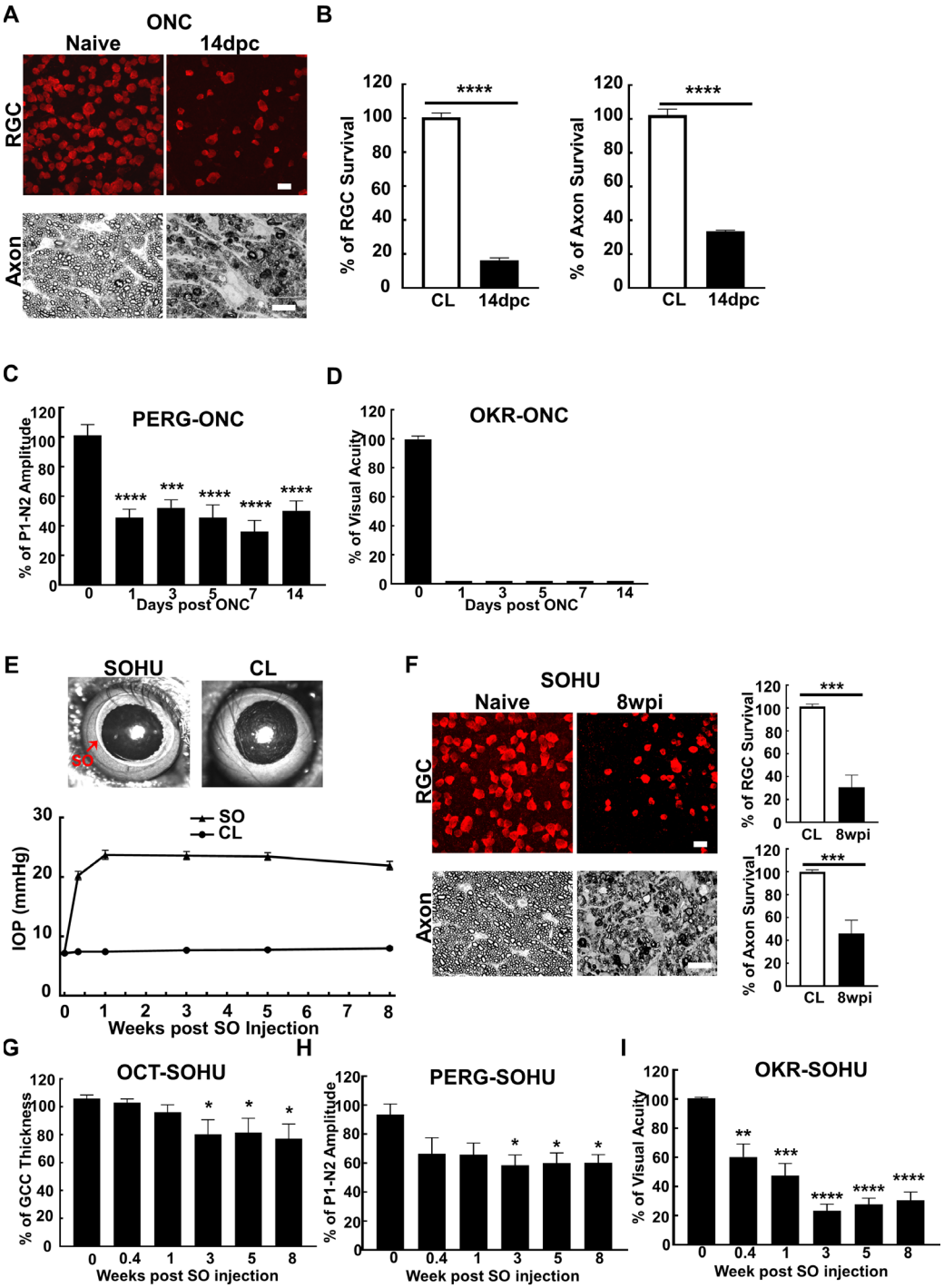

Fig. S3. RGC and optic nerve degeneration and functional deficits in mouse ONC and SOHU glaucoma models. (**A**) Upper panel, confocal images of wholemount retinas showing surviving RBPMS^{+} RGCs; scale bar, 20 μm. Lower panel, light microscope images of semi-thin transverse sections of optic nerve stained with PPD; scale bar, 10 μm.

(**B**) Quantification of surviving RGCs in the peripheral retina and surviving axons in optic nerve at 14dpc, represented as percentage in ONC eyes compared to CL (contralateral) naïve eyes. Data are presented as means ± s.e.m, n = 8. ****: $p<0.0001$. Student's t-test. (**C**) Quantification of P1-N2 amplitude, represented as percentage of P1-N2 amplitude in the ONC eyes, compared to the CL naïve eyes. Data are presented as means ± s.e.m, n = 8. ***: p<0.001, ****: p<0.0001, one-way ANOVA with Tukey's multiple comparisons test. (**D**) Visual acuity measured by OKR, represented as percentage of visual acuity in the ONC eyes, compared to the CL naïve eyes. The visual acuity of the injured eye cannot be detected after ONC. (**E**) Pupillary blocking by SO intracameral injection and IOP elevation at different time points. (**F**) Upper panel, confocal images of wholemount retinas showing surviving $RBPMS^+$ RGCs; scale bar, 20 μm. Lower panel, light microscope images of semi-thin transverse sections of optic nerve stained with PPD; scale bar, 10 μm. Quantification of surviving RGCs in the peripheral retina and surviving axons in optic nerve at 8wpi (weeks post injection), represented as percentage in SOHU eyes compared to CL naïve eyes. Data are presented as means ± s.e.m, n = 7. ***: $p<0.001$. Student's t-test. (**G**) Quantification of GCC thickness acquired by OCT, represented as percentage of GCC thickness in SOHU eyes compared to CL naïve eyes. n = 6 mice. (**H**) Quantification of P1-N2 amplitude, represented as percentage of P1-N2 amplitude in SOHU eyes, compared to CL naïve eyes. n = 6 mice. (**I**) Visual acuity measured by OKR, represented as percentage of visual acuity in SOHU eyes, compared to CL naïve eyes. Data are presented as means ± s.e.m, n = 6. *: p<0.05, **: p<0.01, ***: p<0.001, ****: p<0.0001, one-way ANOVA with Tukey's multiple comparisons test.

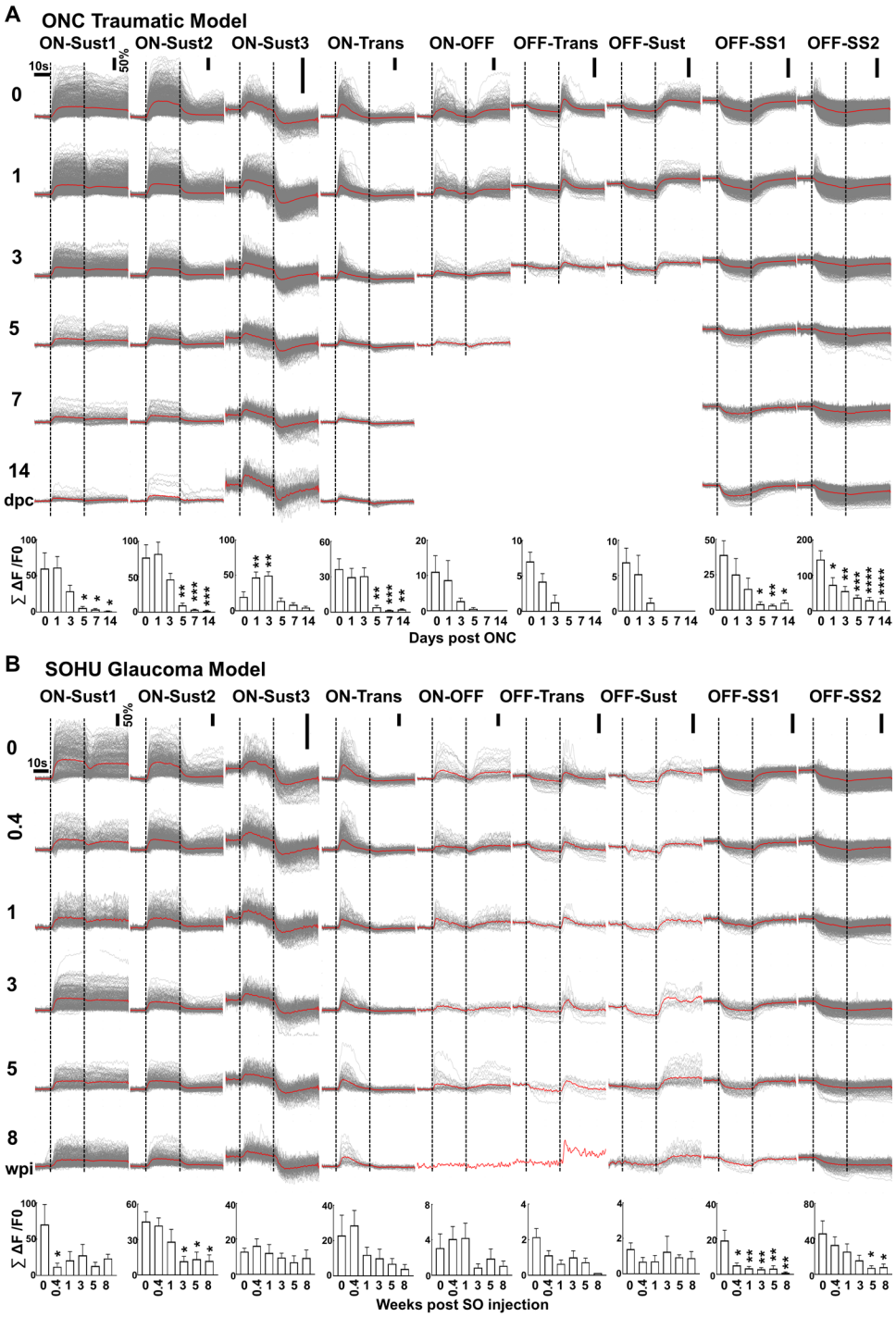

Fig. S4. **Dynamic changes in activity of individual RGC groups in ONC and SOHU glaucoma models.** (**A**) Grey waveform traces are the light-evoked individual RGC responses (ΔF/F0) as a function of time in each RGC functional group at 0, 1, 3, 5, 7, and 14dpc; red line is the mean. Column figures show the total activities of each RGC group,

expressed as the sum of the corresponding group of RGCs' amplitudes from each animal. Data are presented as means ± s.e.m, n = 8 retinas. (**B**) Grey waveform traces are the light-evoked individual RGC responses (ΔF/F0) as a function of time in each RGC functional group at 0, 0.4, 1, 3, 5, and 8wpi; red line is the mean. Column figures show the total activities of each RGC group, expressed as the sum of the corresponding group of RGCs' amplitudes from each retina. Data are presented as means ± s.e.m, n = 6 retinas. *: $p<0.05$, **: $p<0.01$, ***: $p<0.001$, ****: $p<0.0001$, one-way ANOVA with Tukey's multiple comparisons test.

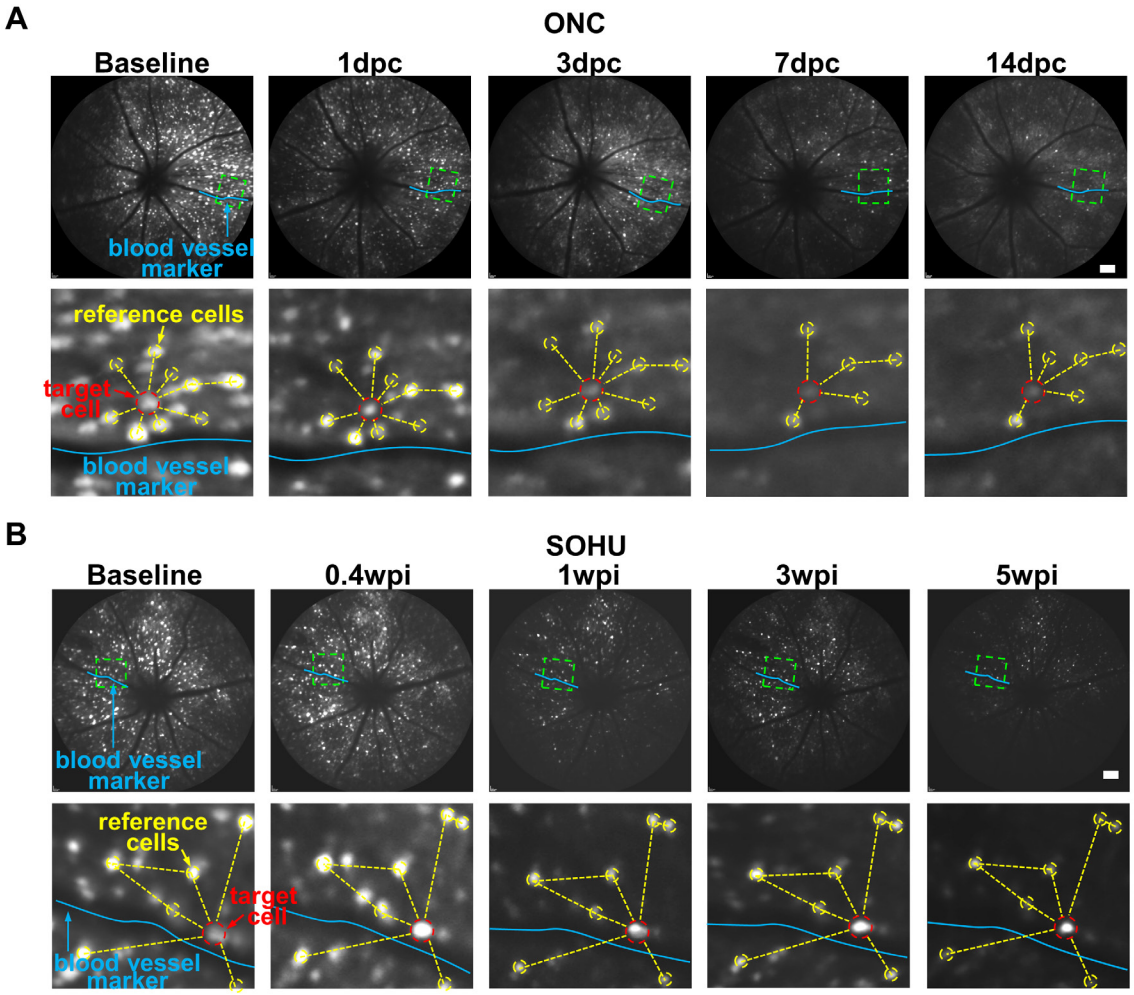

Fig. S5. Longitudinal single RGC tracing in diseased retinas. (**A,B**) cSLO fundus images of the same animal at different time points after injury or diseases and enlarged areas showing blood vessels and surrounding cells as reference points for identifying a target cell.

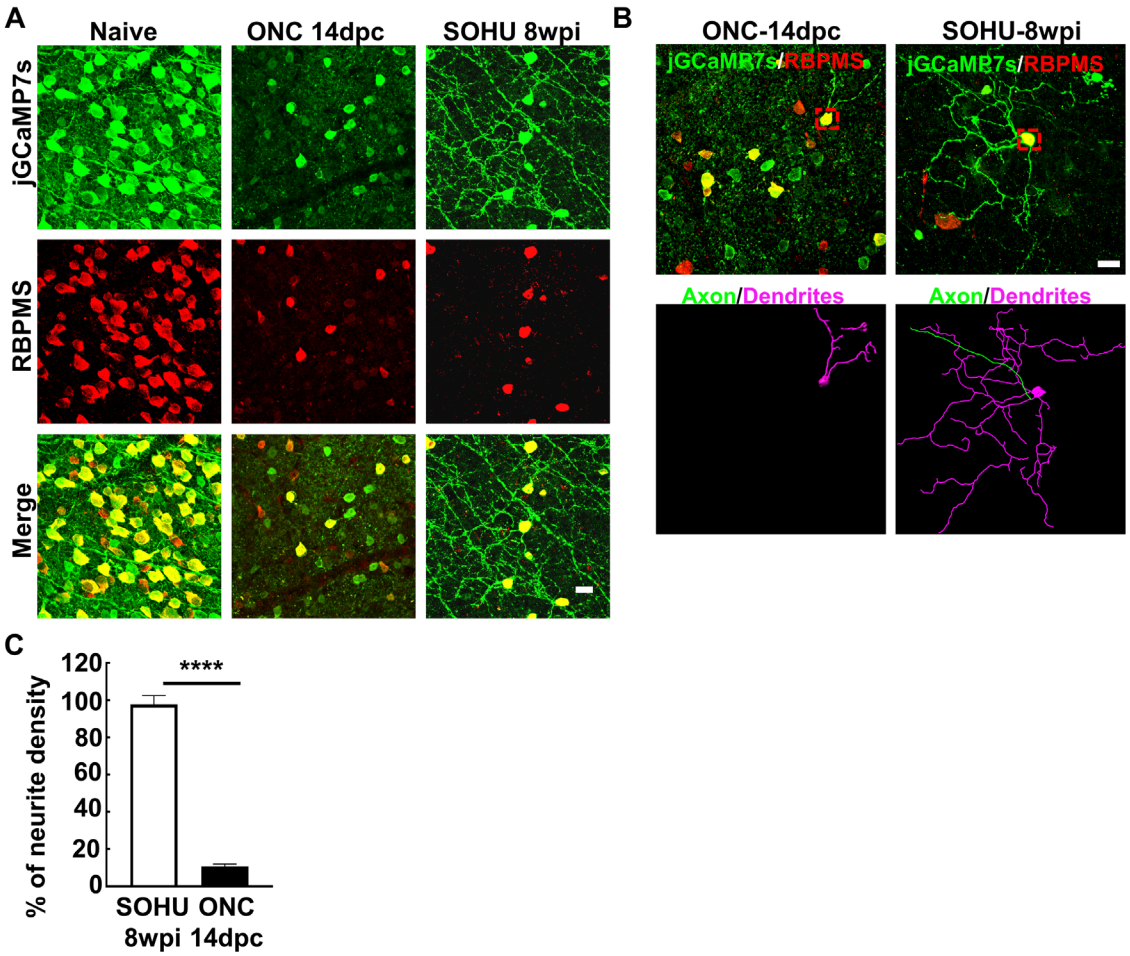

Fig. S6. More dramatic loss of RGC neurites in ONC trauma model than SOHU glaucoma model. (**A**) Confocal images of wholemount retinas showing jGCaMP7s^{+} RGC somata and neurites and RBPMS^{+} RGC somata at 14dpc in ONC and 8wpi in SOHU. The jGCaMP7s signal was augmented by anti-GFP chicken antibodies and secondary donkey anti-chicken antibodies. Scale bar, 20 μm. (B) Representative images showing the outline of RGC neurites at 14dpc and 8wpi. Red dashed boxes are the selected cells shown in the lower panel. Scale bar, 20 μm. (**C**) Quantification of the RGC neurite density at 14dpc in ONC and 8wpi in SOHU, represented as percentage of injured eyes compared to the CL sham eyes. Data are presented as means ± s.e.m, n=20 RGCs of each group. ****: $p<0.0001$. Student's t-test.

Movie S1-3 (separate file).

Movie S1. Videos of *in vivo* Ca^{2+} imaging of a naive mouse fundus during one UV light stimulation cycle (60s).

Movie S2. Videos of *in vivo* Ca^{2+} imaging of representative RGCs from each of the 9 activity groups during one UV light stimulation cycle (60s).

Movie S3. Videos of *in vivo* Ca^{2+} imaging of RGCs in mice at 14dpc (ONC model) or 8wpi (SOHU glaucoma model) during one UV light stimulation cycle (60s).

SI References

1. Q. Wang *et al.*, Mouse gamma-Synuclein Promoter-Mediated Gene Expression and Editing in Mammalian Retinal Ganglion Cells. *J Neurosci* **40**, 3896-3914 (2020).
2. T. J. Atherton, D. J. Kerbyson, Size invariant circle detection. *Image and Vision Computing* **17**, 795-803 (1999).
3. T. Baden *et al.*, The functional diversity of retinal ganglion cells in the mouse. *Nature* **529**, 345-350 (2016).
4. H. Zou, T. Hastie, R. Tibshirani, Sparse Principal Component Analysis. *Journal of Computational and Graphical Statistics* **15**, 265-286 (2006).
5. K. Sjöstrand, L. H. Clemmensen, R. Larsen, G. Einarsson, B. Ersbøll, SpaSM: A MATLAB Toolbox for Sparse Statistical Modeling. *Journal of Statistical Software* **84** (2018).
6. G. McLachlan, and Peel, D., *Finite Mixture Models*, Wiley Series in Probability and Statistics (John Wiley & Sons, Inc., 2000), 10.1002/0471721182.
7. C. Fraley, A. E. Raftery, Model-Based Clustering, Discriminant Analysis, and Density Estimation. *Journal of the American Statistical Association* **97**, 611-631 (2002).
8. L. v. d. M. a. G. Hinton, Visualizing Data using t-SNE. *Journal of Machine Learning Research* **9**, 2579-2605 (2008).
9. L. Yang *et al.*, The mTORC1 effectors S6K1 and 4E-BP play different roles in CNS axon regeneration. *Nature communications* **5**, 5416 (2014).
10. L. Miao *et al.*, mTORC1 is necessary but mTORC2 and GSK3beta are inhibitory for AKT3-induced axon regeneration in the central nervous system. *eLife* **5**, e14908 (2016).
11. H. Huang *et al.*, AKT-dependent and -independent pathways mediate PTEN deletion-induced CNS axon regeneration. *Cell death & disease* **10**, 203 (2019).
12. J. Zhang *et al.*, A Reversible Silicon Oil-Induced Ocular Hypertension Model in Mice. *Journal of visualized experiments : JoVE* **153** (2019).
13. J. Zhang *et al.*, Silicone oil-induced ocular hypertension and glaucomatous neurodegeneration in mouse. *eLife* **8** (2019).
14. F. Fang *et al.*, Chronic mild and acute severe glaucomatous neurodegeneration derived from silicone oil-induced ocular hypertension. *Scientific reports* **11**, 9052 (2021).
15. L. Li *et al.*, Longitudinal Morphological and Functional Assessment of RGC Neurodegeneration After Optic Nerve Crush in Mouse. *Frontiers in cellular neuroscience* **14**, 109 (2020).